Biometals (2012) 25:193–202
DOI 10.1007/s10534-011-9497-3

The influence of reaction temperature on biomineralization of ferrihydrite cores in human H-ferritin

Lanxiang Tian · Changqian Cao · Yongxin Pan

Received: 28 November 2010 / Accepted: 19 September 2011 / Published online: 22 October 2011

Abstract Ferritin is not only important for iron storage and detoxification in living organisms, but a multifunctional size-constrained nanoplatform for biomimetic nanoparticles. In order to tailor the biomimetic nanoparticles for future applications, it is essential to investigate the effects of external factors such as temperature on the particle size and structure of reconstituted cores in ferritin. In this study, we systematically investigated the mineral composition, crystallinity, and particle size of human H-ferritin (HuHF) reconstituted at four different temperatures (25, 30, 37, and 42°C) by integrated magnetic and transmission electron microscopy analyses. Our results showed that the particle size of reconstituted ferrihydrite cores ($\sim$5 nm) in HuHF was temperature-independent. However, the significant changes of the induced magnetization at 5 T field (M_{5T}) and remanent magnetization (M_r) at 5 K clearly showed that the crystallinity of reconstituted cores increased with increasing temperature, indicating that the reaction temperature deeply affects the structural order of reconstituted ferrihydrite cores rather than the particle size, and the reconstituted cores become more ordered at higher reaction temperatures. Our findings provide useful insights into biomineralization of ferritin under in vivo fever condition as well as in biomimetic synthesis of nanomaterials using ferritin. Furthermore, the rock magnetic methods should be very useful approaches for characterizing finite ferritin nanoparticles.

Keywords HuHF · Biomineralization · Biomimetic synthesis · Temperature · Particle size · Degree of crystallinity

L. Tian (✉) · C. Cao · Y. Pan
Paleomagnetism and Geochronology Laboratory, Key Laboratory of the Earth's Deep Interior, Institute of Geology and Geophysics, Chinese Academy of Sciences, 100029 Beijing, People's Republic of China
e-mail: tianlx@mail.iggcas.ac.cn

L. Tian · C. Cao · Y. Pan
Franco-Chinese Biomineralization and Nano-structures Laboratory, Chinese Academy of Sciences, 100029 Beijing, People's Republic of China

Introduction

Ferritin, an iron-storage protein, is ubiquitously distributed in animals, plants, and bacteria, and plays a crucial role in iron storage and detoxification for cellular iron homeostasis. It is composed of a cage-like protein shell and an inorganic iron core. The cage-like three-dimensional structure of ferritin is well conserved throughout living organisms. There are several narrow channels transversing the shell which facilitate inorganic or organic ions to enter and exit the protein cavity. The ferroxidase centers in heavy (H) subunits of ferritin play a critical role particularly in the early stages of iron oxidation and mineralization. Nucleation sites exist in the inner cavity surface involved in

iron core formation. Under in vivo physiological conditions, excessive toxic free iron(II) are sequestered into ferritin cavities to form a biomineralized ferrihydrite core (Arosio et al. 2009; Chasteen and Harrison 1999; Harrison and Arosio 1996). In addition, a new ferrihydrite core can be reconstituted in the apoferritin (metal-free) cavity by in vitro reconstitution, which resembles the natural core (Bielig and Bayer 1955; Macara et al. 1972; Towe and Bradley 1967). Therefore, the in vitro reconstitution has been becoming a major pathway to mimic the in vivo biomineralization mechanisms of ferritin.

Due to being highly homogenous in size, ferritin has been widely used to synthesize a variety of metallic nanomaterials through in vitro biomimetic reconstitution, such as FeS (Douglas et al. 1995; Meldrum et al. 1991), FeOOH (St Pierre et al. 1996), Mn_3O_4 (Meldrum et al. 1995), CoOOH, and Co_3O_4 (Douglas and Stark 2000; Tsukamoto et al. 2005), $Cr(OH)_3$ and $Ni(OH)_3$ (Okuda et al. 2003), CdSe (Yamashita et al. 2004), Pd (Ueno et al. 2004), Ag (Kramer et al. 2004), and CoPt (Warne and Mayes 2003). Compared to the nanoparticles produced by chemical or physical methods, these biomimetic ferritin nanoparticles have advantages of controlled size and shape, monodispersion, and biocompatibility (Meldrum and Cölfen 2008).

To understand the biomineralization or biomimetic mechanisms of ferritin, in vitro reconstitution of ferrihydrite core has been widely studied. Besides protein itself, previous studies have shown that many reaction parameters can affect the biomineralization of ferritin, such as pH, oxiding agents, buffer species, iron concentrations, and buffer concentrations, etc. (Harrison et al. 1967; Macara et al. 1972; Pâques et al. 1980). However, so far, only a few studies have investigated the effect of reaction temperature on the biomineralization of ferritin cores despite it being one of the main determining factors in biomimetic syntheses. The structure of reconstituted ferritin cores from horse spleen were comparatively investigated from low temperatures (4°C, 25°C) to high temperatures (50°C, 55°C) (Chua-Anusorn et al. 2002; St. Pierre et al. 1996). However, the reaction temperatures involved in the two studies are extremely low (4°C) or high (50/55°C) for most living organisms. The effect of temperature between 25°C and 42°C, which is proper to the majority of the biological organisms, on the structure and particle size of reconstituted cores in ferritin is still not clear. Furthermore, 42°C is the maximum body temperature for fever in humans. The effect of high body temperature in vivo on the biomineralization of ferritin is also unclear.

In the present study, we carried out low-temperature magnetic measurements and transmission electron microscopy (TEM) analyses to investigate the size and structure of ferritin cores reconstituted at 25, 30, 37, and 42°C. This study will help us tailor the biomimetic syntheses of ferritin in vitro and improve our understanding of the high body temperature effect on biomineralization of ferritin in vivo.

Materials and methods

The recombinant plasmid pET12b-*HuHF*, which contains the sequence coding the HuHF, was transformed into *Escherichia coli* strain Rosetta. The protein expression and purification were carried out according to the procedure outlined by Santambrogio et al. (2000). The purity of the protein was examined by sodium dodecyl sulfate polyacrylamide gel electrophoresis (SDS-PAGE). The protein concentration was determined by BCA protein assay reagent (Pierce) with bovine serum albumin as standard.

All ferritins were reconstituted using the same experimental procedure except for the temperature. The new cores in HuHFs were reconstituted using air as oxidant at 25, 30, 37, and 42°C, respectively, according to the procedure modified from Wade et al. (1991). The solution of 0.1 M MOPS buffer (pH 7.5) with HuHF (0.5 mg/ml) was added to the reaction vessel. The pH value was stabilized at pH 7.5 using 0.05 M NaOH with a pH stat titrator (842 Titrando, Metrohm). In our preliminary studies, we found that the pH values were not stable through the reconstitution process when using only the MOPS buffer (pH 7.5) as suggested by previous reconstitution experiments (Chua-Anusorn et al. 2002; St. Pierre et al. 1996), because much H^+ was produced. Therefore, all reactions in this study were performed in a pH-stable condition (pH 7.5 $\pm$ 0.01), which was strictly controlled by 0.1 M MOPS buffer and an automated pH stat titration system.

The temperature of the vessel was maintained using an electro-thermostatic water bath ($\pm$0.5°C) (JinTan, China). A solution of 0.0125 M Fe(II) [$(NH_4)_2Fe(SO_4)_2{\cdot}6H_2O$] was added at a flow rate of 50 Fe/protein/min using a dosing device (800 Dosino) connected with 842 Titrando after the water bath reached the required

temperature. After adding theoretical 1,500 Fe/protein into the reaction vessel, the reaction was allowed to continue for 10 more minutes before being stopped. Finally, 200 μl of 0.3 M sodium citrate was added to chelate any free ferrous ions. The reconstituted HuHFs were further purified and concentrated using Microcon Ultrafilters (Millipore) with a 100-kD cut-off. The post-synthesis separation method established in our previous report (Cao et al. 2010) was used to obtain monodispersed reconstituted HuHFs, which is ideal for magnetic characterization and TEM analysis. Samples were freeze-dried to prevent alteration.

For the TEM analysis, reconstituted HuHFs were deposited on ultra-thin carbon-coated copper grids. TEM observations were performed on a JEOL2010 TEM operating at 200 kV. Selected area electron diffraction (SAED) patterns were recorded. The average particle sizes were determined by measuring 800 particles of each sample of reconstituted HuHFs. Statistical analyses were performed using SPSS for Windows 13.0 (SPSS Inc. Chicago, IL, USA).

Due to the low crystallinity and/or small particle size, the magnetic properties are very useful for characterizing the structure of ferrihydrite nanoparticles (Guyodo et al. 2006; Mørup et al. 2007). Low-temperature magnetic measurements were performed on a Quantum Design MPMS SQUID magnetometer (Model XP-5XL, with magnetic moment sensitivity of 5.0×10^{-10} Am^2). The acquisition of isothermal remanent magnetization (IRM) up to 5 T and DC demagnetization (DCD) data were measured at 5 K to evaluate the influence of magnetostatic interactions. Hysteresis loops were measured between ±5 T at 5 K. Low-field magnetization curves were measured between 5 and 300 K in a field of 5 mT, after the sample was cooled to 5 K in zero-field (zero-field cooling, ZFC) and after cooling in a 5-mT field (field-cooling, FC). The thermal decay curves of isothermal remanence acquired at 5 K in a field of 5 T after cooling in ZFC and a 5 T FC were measured between 5 and 300 K as well.

Results

TEM analyses

The resulting solutions were found to be clear, with a reddish brown color. No precipitation was observed even after centrifugating the reconstituted HuHFs for 20 min at 10,000 × *g*. TEM observations showed that the reconstituted HuHFs at 25, 30, 37, and 42°C had monodispersed electron-dense near-spherical cores. The SAED patterns of the four reconstituted samples were indistinguishable and consisted of four major rings corresponding to the *d* spacings of 0.25, 0.22, 0.17, and 0.15 nm. Representative image and SAED patterns of the 42°C reconstituted HuHF sample are shown in Fig. 1, which indicated that the core compositions in the reconstituted cores of HuHFs were ferrihydrite. We further investigated the subtle structural differences of cores reconstituted under different temperatures using high-resolution TEM (Fig. 2). The majority of 25°C_HuHF cores appear amorphous structure with a few faintly visible lattice fringes (Fig. 2a), while the other three samples had some identifiable lattice fringes. There were amorphous structure and lattice fringes co-occurrence in one core (Fig. 2b–d). It is hard to differentiate the crystallinity of ferritins cores reconstituted at four temperatures using high-resolution TEM.

The particle-size distributions of the reconstituted HuHF ferrihydrite cores can be approximated by normal distributions with low standard deviations (Q–Q plot). The mean diameters of ferrihydrite cores were 5.5 ± 0.7, 5.0 ± 0.7, 5.2 ± 0.8, and 4.9 ± 0.8 nm for 25, 30, 37, and 42°C HuHFs samples, respectively (Fig. 3).

Magnetostatic interactions

Since magnetostatic interactions strongly affect the magnetic properties (Berquo et al. 2009; Mørup et al. 2007; Prené et al. 1994), magnetostatic interactions between reconstituted HuHF ferrihydrite cores were evaluated using Wohlfarth–Cisowski test (Cisowski 1981; Wohlfarth 1955) and Henkel-plot (Henkel 1964). Results were shown in Fig. 4. The I_d (H) curve has been rescaled as $0.5\ (1 + I_d\ (H))/M_{5T}$, and the Henkel plot, [$I_r$ (H)] versus [I_d (H)], was normalized by M_{5T}. The R values of Wohlfarth-Cisowski test for the four reconstituted HuHFs were 0.5, and the corresponding Henkel plots are linear, which indicate nearly no magnetostatic interactions between ferrihydrite cores. It should be noted that the four samples were

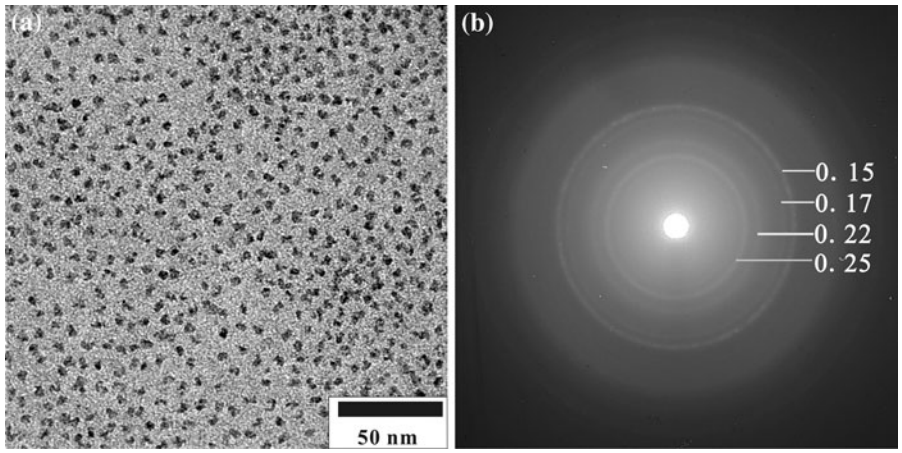

Fig. 1 TEM micrograph (**a**) and SAED pattern (**b**) of HuHF reconstituted at 42°C

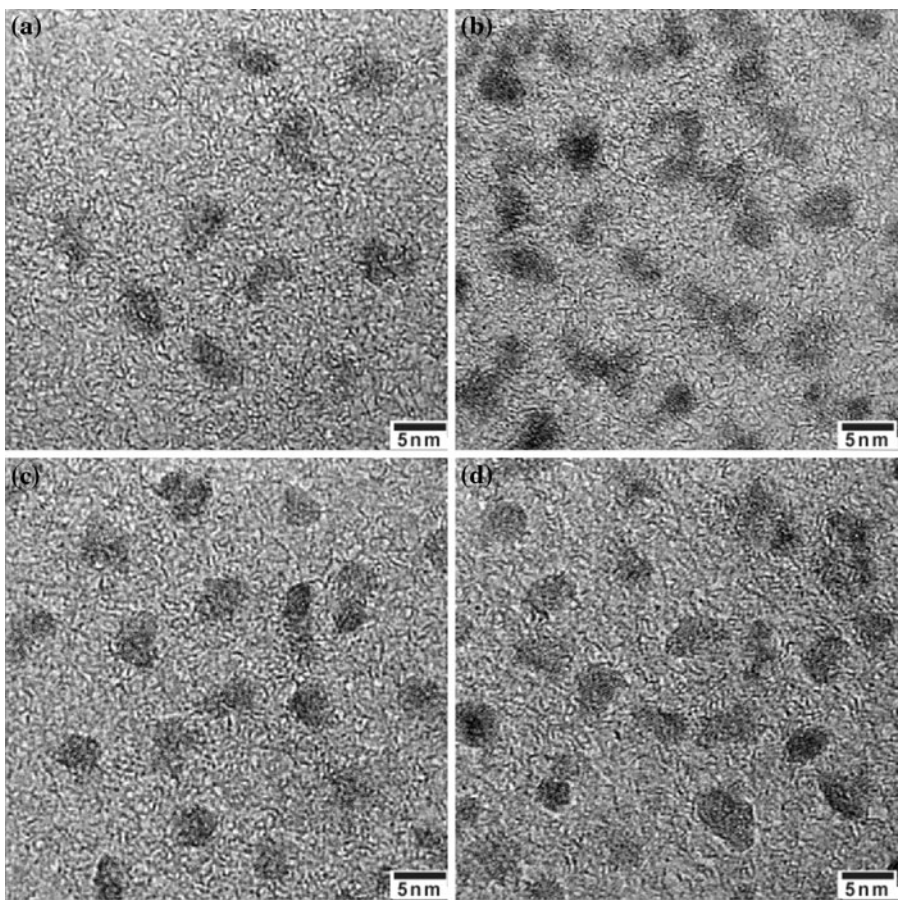

Fig. 2 The high-resolution TEM images of reconstituted ferritins at 25, 30, 37, and 42°C. *Scale bar* is 5 nm

not saturated even in the highest applied field (5 T) at 5 K. The median destructive field, i.e., the value of field for which one-half the initial remanence is lost, for the four samples is approximately 0.69 T (Fig. 4), confirming the hard coercivity of ferrihydrite cores.

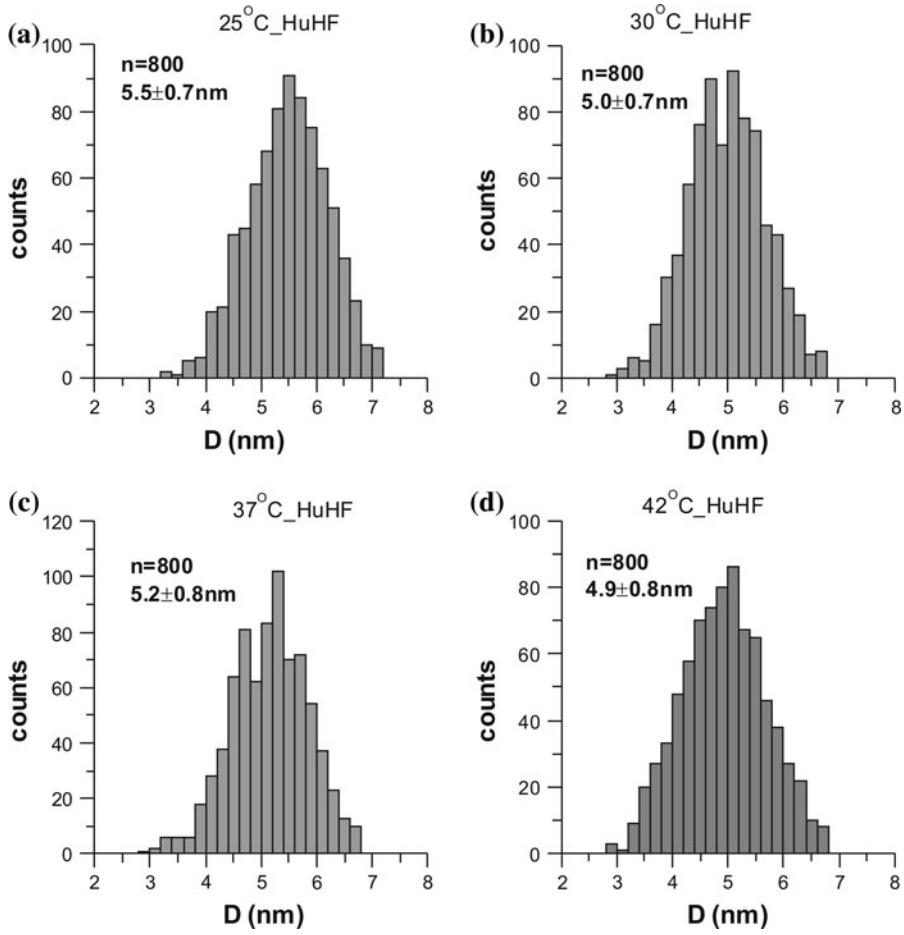

Fig. 3 The size histograms of the four reconstituted HuHF samples (**a**–**d**)

Hysteresis loops

As shown in Fig. 5, all samples were clearly not saturated up to 5 T, which indicated the high coercivity of ferrihydrite cores. The H_{cr} of the four reconstituted HuHFs ferrihydrite cores was ≥0.69 T (Fig. 5; Table 1), much higher than that of the H_{cr} (~35 mT) for ferrimagnetic HuHFs (Cao et al. 2010). The surface-uncompensated moments of ferrihydrite nanoparticles might contribute to the non-saturation trend (Allen et al. 1998; Papaefthymiou 2010). The wasp-waisted shape of the hysteresis loops was due to the mixture of single-domain (SD) particles and superparamagnetic (SP) particles at the measured temperature of 5 K (Roberts et al. 1995; Tauxe et al. 1996; Tian et al. 2010).

Both M_r and M_{5T} of the four reconstituted HuHFs tended to decrease with increasing reaction temperature (Pearson correlation, $r = -0.97$, $p < 0.05$). The ratio M_r/M_{5T}, H_c, and H_{cr}, however, remain constant (Table 1).

Low-field magnetization curves

For monodispersed non-interacting particles, the ZFC magnetization curve has a maximum at the blocking temperature (Mørup et al. 2007). According to $KV = k_B T_b \ln(\tau_m/\tau_0)$, where K is the magnetic anisotropy energy constant, k_B is the Boltzmann constant, τ_0 is the characteristic time of thermal fluctuations, and τ_m is the measuring time, the T_b can be used to estimate the average particle volume of a sample, V (Dunlop and Özdemir 1997; Tartaj 2009). As shown in Fig. 6a–d, the T_b of reconstituted HuHFs samples was 10 K for all four samples, supporting the TEM results that the volumes of ferritin cores did not change under different reaction temperatures. The ZFC and FC curves merged at 12 K, which corresponds to the

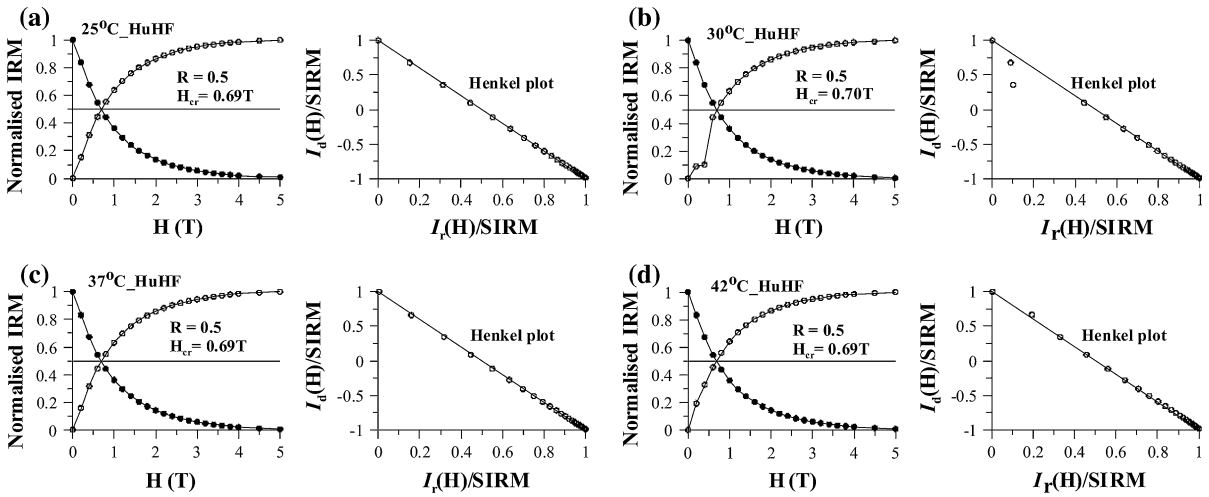

Fig. 4 The Wohlfarth-Cisowski test and Henkel-plot curves of the four reconstituted HuHFs measured at 5 K. The *solid line* on the Henkel-plot is from the Wohlfarth theory for non-interacting systems

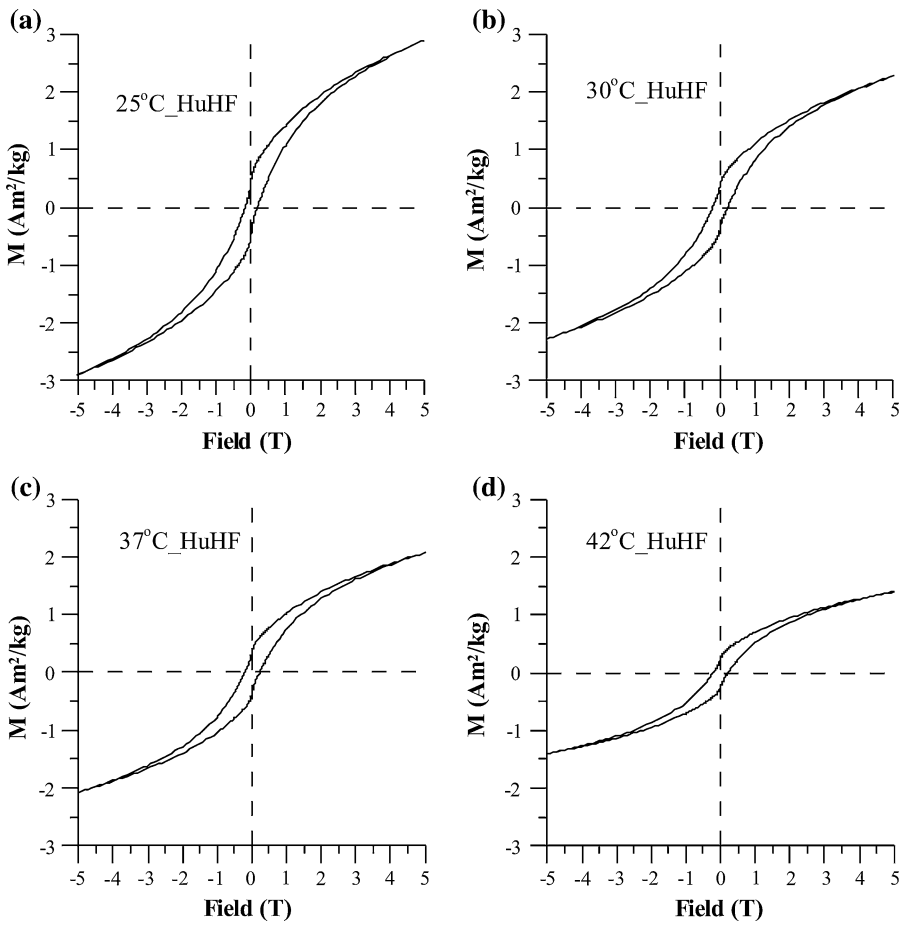

Fig. 5 Hysteresis loops from the four reconstituted HuHFs measured at 5 K (without paramagnetic correction)

Table 1 Magnetic hysteresis parameters of the four reconstituted HuHF samples

Samples	M_r (Am^2/kg)	M_{5T} (Am^2/kg)	M_r/M_{5T}	H_{cr} (T)	H_c (T)
25°C_HuHF	0.49	2.90	0.17	0.69	0.18
30°C_HuHF	0.40	2.28	0.18	0.70	0.21
37°C_HuHF	0.34	2.08	0.16	0.69	0.21
42°C_HuHF	0.23	1.40	0.16	0.69	0.21

maximum unblocking temperature; this suggested a very narrow particle size distribution. In contrast, the initial magnetization in FC curve decreased with increasing synthesis temperature.

Remanence decay curves

The IRM_{5T_5K} in ZFC and FC curves appeared to decrease with increasing synthesis temperatures, similar to the trends in low-field magnetization curve and the magnetization values acquired in hysteresis loops at 5 K (Fig. 6e–h). The IRM_{5T_5K} values for the FC curves were 0.51, 0.41, 0.40, and 0.28 Am^2/kg for 25, 30, 37, and 42°C HuHFs samples, respectively. The thermal demagnetization curves of IRM_{5T_5K} acquired at 5 K had a rapid decay of remanence below 16 K, which was due to single-domain particles unblocking into a superparamagnetic state with increasing temperature. The temperature at which the remanence is removed in the ZFC curve corresponds to the maximum blocking temperature (T_{max}). At this temperature all particles are unblocked. The T_{max} values in the FC curves were 16.3, 16.2, 17.2, and 17.1 K for 25, 30, 37, and 42°C HuHFs samples, respectively. This narrow range of T_{max} further indicated that the four samples had similar grain-size distributions.

Discussion

In this study, the equal T_b of the four reconstituted HuHFs at 25, 30, 37, and 42°C clearly indicated that the average particle sizes of the four HuHFs were the same, which was identical to the result of diameters statistical analyses from the TEM data. The SAED analyses and magnetic measurements showed that the

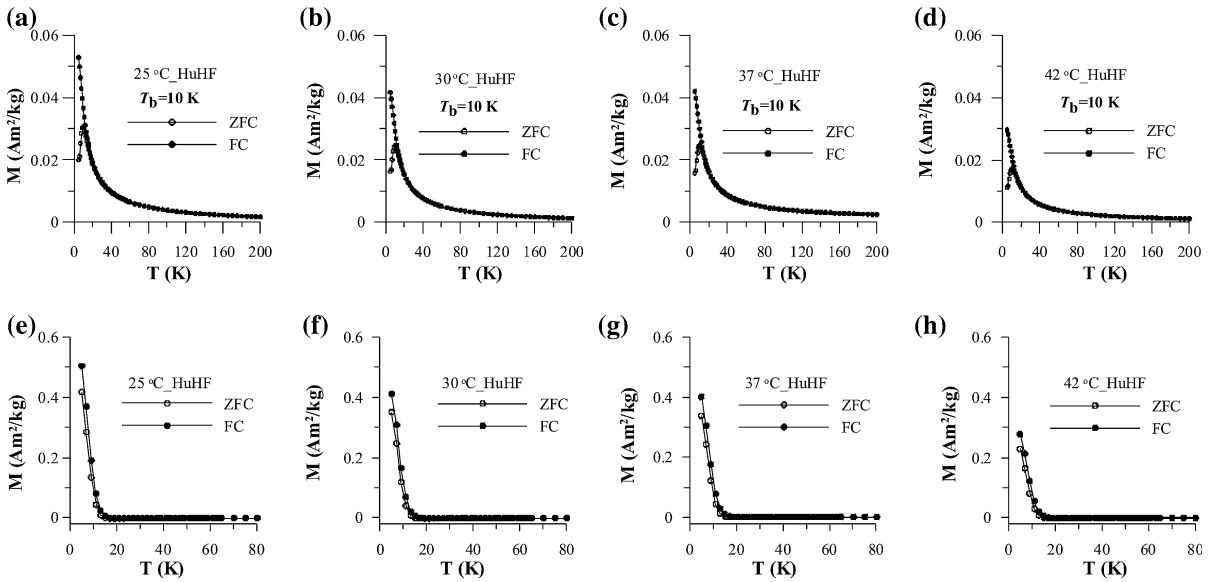

Fig. 6 Low-field (5 mT) magnetization curves as a function of temperature measured after zero-field-cooling (ZFC) and filed-cooling (FC) treatments for the four reconstituted HuHFs (**a**–**d**). The decay curves of remanent magnetization acquired in a 5-T applied field after zero-field-cooling (ZFC) and field-cooling (FC) treatments for the four reconstituted HuHFs (**e**–**h**)

mineral phases of reconstituted ferritins were ferrihydrite. This is consistent with previous reports (Rohrer et al. 1990; St. Pierre et al. 1996; Wade et al. 1993). High-resolution TEM images showed that more crystals appeared in the other three reconstituted HuHFs, except for the 25°C_HuHF. However, for the ~5-nm ultrafine nanoparticles, it is hard to quantitatively distinguish the differences of the crystallinity among the HuHFs reconstituted at 30, 37, and 42°C by high-resolution TEM images.

The induced magnetization (M_{5T}) and remanent magnetizations (M_r and IRM_{5T_5K}) decreased with increasing reaction temperatures, which strongly suggests that the degree of crystallinity of reconstituted HuHFs cores is enhanced with increasing reaction temperatures. The size, structure, and mineral composition of crystals can affect the values of M_{rs}, M_{5T}, H_c, and H_{cr} (Dunlop and Özdemir 1997). The observed changes in M_{5T} and M_r can be explained by a superantiferromagnetism model (Gilles et al. 2002). For bulk antiferromagnetic particles, the net magnetization will be zero due to the neighbor sub-lattices with opposite spins. However, when the particles reach the nanometer range, the finite-size effect leads to increasing fraction of atoms lying at the surface with lower atomic coordination than in the core. That is, the contribution of the uncompensated surface spins to the total magnetization of the particle may be larger than that of the core (Pérez et al. 2008). For superantiferromagnetic ferritin, a small net magnetization can be detected in the presence of an external field. The number of uncompensated surface spins is closely related to the particle size and the degree of crystallinity (Mørup et al. 2007). In this study, the effect of particle size can be excluded since ferritins almost have identical average particle sizes based on TEM observation (Fig. 3) and low-field magnetization results (Fig. 6). Therefore, the degree of crystallinity contributes mostly to our sample. The relative number of uncompensated surface spins of HuHF cores is expected to decrease with increasing crystallinity of the ferrihydrite cores (with high atomic coordination) and the net magnetization of ferrihydrite will decrease (Guyodo et al. 2006; Zergenyi et al. 2000). The H_c, H_{cr}, and M_{rs}/M_{5T} of the four reconstituted HuHFs are basically equal, since these magnetic parameters are more prone to be affected by particle size than the crystal structure of ferritin-like nanoparticles.

Temperature plays a major role in ferrous ions dispersion and transferring to the inner cavity of ferritin. Higher temperatures could facilitate the stacking of atoms in an orderly fashion and form a crystalline lattice (Cushing et al. 2004; St. Pierre et al. 1996). The dosing rate of iron is also an important factor for iron incorporation into protein. Previous experiments have shown that the reaction rate of HuHF is the fastest one among the different ferritins (HuHF > HoSF > HuLF), and the incorporation reaction of 33 Fe^{2+}/HuHF rapidly completed within 25 s at 20°C (Yang et al. 1998). In this study, under the dosing rate of 50 Fe/(protein·min), no precipitation out of proteins is observed in the resulting solutions and the average particle sizes of four reconstituted ferritins are basically equal. This evidence indicates that the dosing rate of 50 Fe(II)/protein/minute is not a fast rate for HuHF reconstitution and nearly all of the iron should be incorporated by HuHF even at lower temperature (25°C in this study). Despite the different ferritin templates, the result of human H-ferritin in this study is similar to the results of horse spleen ferritin in previous studies. The degree of crystallinity of reconstituted cores increases with increasing reaction temperatures (Chua-Anusorn et al. 2002; St. Pierre et al. 1996), which indicates that the effect of temperature on structure of reconstituted cores could extend to all other source ferritins.

Our results suggest that reconstituted cores with high ordered structure can be tailored by increasing reaction temperature in biomimetic syntheses. Compared to the 37°C_HuHF, the 42°C_HuHF has a more ordered structure, which indicates that fever in the human body could affect the biomineralization of ferritin in vivo.

Conclusions

The mineral phases of the reconstituted HuHFs synthesized at 25, 30, 37, and 42°C in this study are all ferrihydrite. The degree of crystallinity of the HuHF cores increases with increasing reaction temperatures (42°C_HuHF has a higher crystallinity than 37°C_HuHF) without influence on the average particle size. This implies that high body temperature during long-period fever could affect the structure of ferritin in vivo.

Acknowledgments This work was supported by the National Natural Science Foundation of China (No. 40821091 and 40904017), the CAS/SAFEA International Partnership Program for Creative Research Teams (KZCX2-YW-T10) and China Postdoctoral Science Foundation. The authors are grateful to Paolo Arosio for providing us the vector pET12b-encoded cDNA of human H chain ferritin. The authors gratefully acknowledge the anonymous reviewers for very careful review and very constructive comments, Dr. Qingsong Liu and Jinhua Li for helping magnetic data analysis, and Dr. G.A. Paterson for improving the writing of this manuscript.

References

Allen PD, St Pierre TG, Street R (1998) Magnetic interactions in native horse spleen ferritin below the superparamagnetic blocking temperature. J Magn Magn Mater 177:1459–1460

Arosio P, Ingrassia R, Cavadini P (2009) Ferritins: a family of molecules for iron storage, antioxidation and more. Biochim Biophys Acta 1790:589–599

Berquo T, Erbs J, Lindquist A, Penn R, Banerjee S (2009) Effects of magnetic interactions in antiferromagnetic ferrihydrite particles. J Phys Condes Matter 21(17):176005

Bielig HJ, Bayer E (1955) Eisenaustausch Zwischen Proteiner-Modellversuche Zur Eisenresorption Und Speicherung Im Tierkorper. Naturwissenschaften 42(16):466

Cao CQ, Tian LX, Liu QS, Liu WF, Chen GJ, Pan YX (2010) Magnetic characterization of non-interacting, randomly oriented, nanometer-scale ferrimagnetic particles. J Geophys Res 115:B07103. doi:10.1029/2009JB006855

Chasteen ND, Harrison PM (1999) Mineralization in ferritin: an efficient means of iron storage. J Struct Biol 126: 182–194

Chua-Anusorn W, Mun H-R, Webb J, Gorham NT, St. Pierre TG (2002) Effect of precipitation temperature and number of iron atoms per molecule on the structure of hydrated iron(III) oxyhydroxide ferritin cores synthesised in vitro. Hyperfine Interact 144(145):279–288

Cisowski S (1981) Interacting versus non-interacting single domain behavior in natural and synthetic samples. Phys Earth Planet Inter 26(1–2):56–62

Cushing BL, Kolesnichenko VL, O'Connor CJ (2004) Recent advances in the liquid-phase syntheses of inorganic nanoparticles. Chem Rev 104:3893–3946

Douglas T, Stark VT (2000) Nanophase cobalt oxyhydroxide mineral synthesized within the protein cage of ferritin. Inorg Chem 39(8):1828–1830

Douglas T, Dickson DPE, Betteridge S, Charnock J, Garner CD, Mann S (1995) Synthesis and structure of an iron(III) sulfide-ferritin bioinorganic nanocomposite. Science 269(5220): 54–57

Dunlop DJ, Özdemir Ö (1997) Rock magnetism-fundamentals and frontiers. Cambridge University Press, Cambridge

Gilles C, Bonville P, Rakoto H, Broto JM, Wong KKW, Mann S (2002) Magnetic hysteresis and super antiferromagnetism in ferritin nanoparticles. J Magn Magn Mater 241(2–3): 430–440

Guyodo Y, Banerjee SK, Penn RL, Burleson D, Berquo TS, Seda T, Solheid P (2006) Magnetic properties of synthetic six-line ferrihydrite nanoparticles. Phys Earth Planet Inter 154:222–233

Harrison PM, Arosio P (1996) The ferritins: molecular properties, iron storage function and cellular regulation. Biochim Biophys Acta 1275:161–203

Harrison PM, Fischbach FA, Hoy TG, Haggis GH (1967) Ferric oxyhydroxide core of ferritin. Nature 216:1188–1190

Henkel O (1964) Remanenzverhalten und wechselwirkungen in hartmagnetischen teilchenkollektiven. Phys Status Solidi B 7(3):919–929

Kramer RM, Li C, Carter DC, Stone MO, Naik RR (2004) Engineered protein cages for nanomaterial synthesis. J Am Chem Soc 126(41):13282–13286

Macara IG, Hoy TG, Harrison PM (1972) The formation of ferritin from apoferritin. Biochem J 126:151–162

Meldrum FC, Cölfen H (2008) Controlling mineral morphologies and structures in biological and synthetic systems. Chem Rev 108(11):4332–4432

Meldrum FC, Wade VJ, Nimmo DL, Heywood BR, Mann S (1991) Synthesis of inorganic nanophase materials in supramolecular protein cages. Nature 349(21):684–687

Meldrum FC, Douglas T, Levi S, Arosio P, Mann S (1995) Reconstitution of manganese oxide cores in horse spleen and recombinant ferritins. J Inorg Biochem 58:59–68

Mørup S, Madsen DE, Frandsen C, Bahl CRH, Hansen MF (2007) Experimental and theoretical studies of nanoparticles of antiferromagnetic materials. J Phys Condes Matter 19:213202

Okuda M, Iwahori K, Yamashita I, Yoshimura H (2003) Fabrication of nickel and chromium nanoparticles using the protein cage of apoferritin. Biotechnol Bioeng 84(2): 187–194

Papaefthymiou GC (2010) The Mössbauer and magnetic properties of ferritin cores. Biochim Biophys Acta 1800(8): 886–897

Pâques EP, Pâques A, Crichton RR (1980) A study of the mechanism of ferritin formation-the effect of pH, ionic strength and temperature, inhibition by imidazole and kinetic analysis. Eur J Biochem 107:447–453

Pérez N, Guardia P, Roca AG, Morales MP, Serna CJ, Iglesias O, Bartolomé F, García LM, Batlle X, Labarta A (2008) Surface anisotropy broadening of the energy barrier distribution in magnetic nanoparticles. Nanotechnology 19:475704

Prené P, Tronc E, Jolivet JP, Livage J, Cherkaoui R, Noguès M, Dormann JL (1994) Mössbauer investigation of non-aggregated γ-Fe_20_3 particles. Hyperfine Interact 93: 1409–1414

Roberts AP, Cui Y, Verosub KL (1995) Wasp-waisted hysteresis loops: mineral magnetic characteristics and discrimination of components in mixed magnetic systems. J Geophys Res 100(B9):17909–17924

Rohrer JS, Islam QT, Watt GD, Sayers DE, Theil EC (1990) Iron environment in ferritin with large amounts of phosphate, from *Azotobacter vinelandii* and horse spleen, analyzed using extended X-ray absorption fine structure (EXAFS). Biochemistry 29:259–264

Santambrogio P, Cozzi A, Levi S, Rovida E, Magni F, Albertini A, Arosio P (2000) Functional and immunological analysis of recombinant mouse H- and L-ferritins from *Escherichia coli*. Protein Expr Purif 19(1):212–218

St Pierre TG, Chan P, Bauchspiess KR, Webb J, Betteridge S, Walton S, Dickson DPE (1996) Synthesis, structure and magnetic properties of ferritin cores with varying composition and degrees of structural order: models for iron oxide deposits in iron-overload diseases. Coord Chem Rev 151:125–143

Tartaj P (2009) Super paramagnetic composites: magnetism with no memory. Eur J Inorg Chem 2009(3):333–343

Tauxe L, Mullender TAT, Pick T (1996) Potbellies, wasp-waists, and super paramagnetism in magnetic hysteresis. J Geophys Res 101(B1):571–583

Tian LX, Cao CQ, Liu QS, Pan YX (2010) Low-temperature magnetic properties of horse spleen ferritin. Chin Sci Bull 55(27–28):3174–3180

Towe KM, Bradley WF (1967) Mineralogical constitution of colloidal "hydrous ferric oxides". J Colloid Interface Sci 24(3):384–392

Tsukamoto R, Iwahori K, Muraoka M, Yamashita I (2005) Synthesis of Co_3O_4 nanoparticles using the cage-shaped protein, apoferritin. Bull Chem Soc Jpn 78(11):2075–2081

Ueno T, Suzuki M, Goto T, Matsumoto T, Nagayama K, Watanabe Y (2004) Size-selective olefin hydrogenation by a Pd nanocluster provided in an apo-ferritin cage. Angew Chem-Int Ed Engl 43(19):2527–2530

Wade VJ, Levi S, Arosio P, Treffry A, Harrison PM, Mann S (1991) Influence of site-directed modifications on the formation of iron cores in ferritin. J Mol Biol 221(4):1443–1452

Wade VJ, Treffry A, Laulhere JP, Bauminger ER, Cleton MI, Mann S, Briat JF, Harrison PM (1993) Structure and composition of ferritin cores from Pea Seed (*Pisum-Sativum*). Biochim Biophys Acta 1161(1):91–96

Warne B, Mayes EL (2003) Production of CoPt alloy grains within protein templates. Bioinspired nanoscale hybrid systems. Materials Research Society, Warrendale. pp 171–177

Wohlfarth EP (1955) The effect of particle interaction on the coercive force of ferromagnetic micropowders. Proc R Soc A Math Phys Eng Sci 232(1189):208–227

Yamashita I, Hayashi J, Hara M (2004) Bio-template synthesis of uniform CdSe nanoparticles using cage-shaped protein, apoferritin. Chem Lett 33(9):1158–1159

Yang XK, Barrett YC, Arosio P, Chasteen ND (1998) Reaction paths of iron oxidation and hydrolysis in horse spleen and recombinant human ferritins. Biochemistry 37(27): 9743–9750

Zergenyi RS, Hirt AM, Zimmermann S, Dobson JP, Lowrie W (2000) Low-temperature magnetic behavior of ferrihydrite. J Geophys Res 105(B4):8297–8303